Silica/Polymer TIR Optical Switches and a Proposal for Nonblocking Four-Port Routers

Chuan-Tao Zheng, Lei Liang, Wei-Lin Ye, Da-Ming Zhang, and Chun-Sheng Ma

***Abstract*— We have fabricated a wavelength-insensitive silica/polymer total-internal-reflection thermooptic switch element using photolithography and wet etching techniques. A switching power of 70 mW is required to drop the crosstalk below −20 dB. Under through and reflection states, the propagation losses of the 0.47-cm long core switch element are measured to be 1.8 and 3.6 dB, respectively. The 10%–90% rise time and the 90%–10% fall time are 0.35/0.38 and 0.52 ms, respectively. Using 11 switch elements, we have proposed a nonblocking four-port optical router. The propagation loss range is ∼5.4–23.4 dB along all routing paths. Both the switch and the router show potential applications of wideband signal switching and routing in multiprocessor-based optical networks-on-chip.**

***Index Terms*— Integrated optical device, optoelectronics, optical switching device, optical networks-on-chip.**

I. Introduction

With the fast development of chip-level multiprocessors in networks-on-chip (NoC), a new era has been coming when the processor cores must work in parallel, and interconnection with a large bandwidth, a low latency, and a low power consumption are highly required to utilize the chip's parallel resources. Moreover, because of advances in micro- and nano-scale photonics and photonic devices, photonic NoC, instead of electronic NoC, becomes a promising solution to meet the increasing chip-level interconnection challenges [1].

Since the on-chip photonic interconnection network is composed of passive waveguides and optical routers, design and fabrication of both passive and active optical routers, which are capable of selecting paths between a set of input and output ports, become a hot research issue in recent years. In term of switching elements, microring resonators (MRRs) and Mach-Zehnder interferometers (MZIs) are two common optical structures for constructing four-port [2]–[4], five-port [5], [6], and port-scalable optical routers [7], [8]. They are generally based on the silicon material and its carrier-dispersion-induced electro-optic (EO) effect or thermo-optic (TO) effect.

Compared with other materials such as silica, lithium niobate, and III–V compound semiconductors, polymers offer many unique properties including ease of fabrication, accurate control of refractive index, a low production cost, and compatibility with silicon fabrication technologies [9], [10]. Therefore, as a difference from the ever reported MRR- or MZI-based silicon four-port routers [2]–[4], in this letter, a non-blocking four-port routing scheme is proposed. Though the four-port router has more elements than the recently proposed routing models in [2]–[4], [7], and [8], it shows some differences, including 1) using total-internal-reflection (TIR) switches as basic routing elements, which enables both the switching element and the router to reveal a wide spectrum; 2) a new non-blocking routing network topology different from the reported schemes; 3) using a silica/polymer hybrid waveguide structure and TO effect of polymer, which results in both a low power consumption and a fast response speed due to a high TO coefficient of polymer and a large thermal conductivity of silica.

Manuscript received September 29, 2014; revised December 7, 2014; accepted December 17, 2014. Date of publication December 24, 2014; date of current version February 19, 2015. This work was supported in part by the Science and Technology Department of Jilin Province, China, under Grant 20130522161JH, in part by the Ministry of Education, China, under Grant 20110061120052 and Grant 20120061130008, and in part by the National Science Foundation of China under Grant 61107021, Grant 61177027, and Grant 61077074.

C.-T. Zheng, D.-M. Zhang, and C.-S. Ma are with the State Key Laboratory on Integrated Optoelectronics, College of Electronic Science and Engineering, Jilin University, Changchun 130012, China (e-mail: zhengchuantao@jlu.edu.cn; zhangdm@jlu.edu.cn; mcsheng@163.com).

L. Liang is with the Changchun Institute of Optics, Fine Mechanics and Physics, Chinese Academy of Sciences, Changchun 130012, China (e-mail: lianglei0427@163.com).

W.-L. Ye is with the College of Engineering, Shantou University, Shantou 515063, China (e-mail: wlye@stu.edu.cn).

Color versions of one or more of the figures in this letter are available online at http://ieeexplore.ieee.org.

Digital Object Identifier 10.1109/LPT.2014.2385733

II. Design of TIR TO Switch Elements

A. Device Structure

As a basic routing element, Fig. 1(a) depicts the structure of the 2×2 bidirectional silica/polymer TIR TO switch, which is essentially an X-junction formed by two crossing rib waveguides. There are totally five regions, including (i) input region, (ii) transition region I, (iii) TIR region, (iv) transition region II, and (v) output region. Each waveguide in the TIR region contains three sections, e.g. two taper waveguide sections and one uniform waveguide section with a relatively wide waveguide width for realizing good mode-through and reflection operations. In the two transition regions, four arc-bending waveguides are used.

The rib waveguide adopts silica, SU-8 2005 and P(MMA-GMA) as an under-buffer layer, a core layer and an upper-buffer layer, respectively. The waveguide cross-sectional view in the single-mode input/output region is shown in Fig. 1(b), and that over the waveguide cross-point in the TIR region is shown in Fig. 1(c). For inducing TO effect, a gold electrode heater is deposited in the TIR region. The materials' optical constants at 1550 nm are listed in Table I.

B. Waveguide Design at 1550 nm Wavelength

The input/output waveguides should assure that only the E_{00}^{y} fundamental mode can propagate in them. Under the thicknesses of the layers shown in Fig. 1(b), Fig. 2(a) exhibits the calculated effective refractive index and amplitude loss coefficient of each mode versus rib waveguide width a_1.

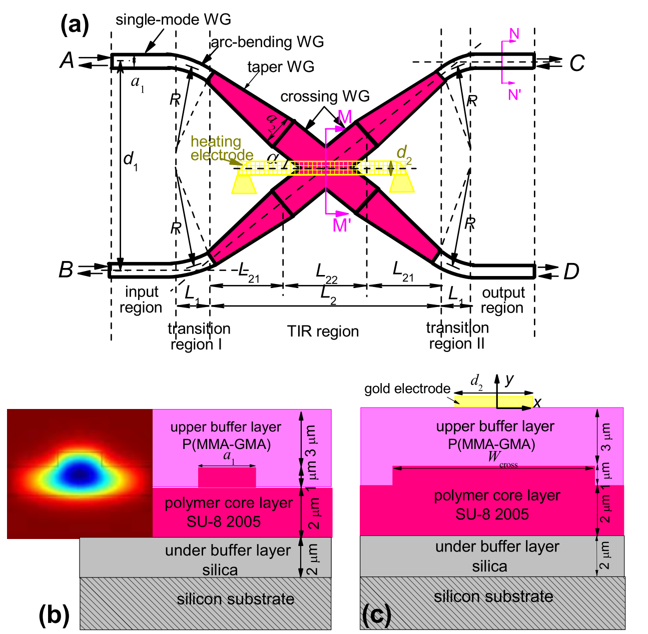

Fig. 1. (a) Schematic diagram, (b) cross-sectional view NN' in the input/output region, and (c) cross-section view MM' over the cross-point in the TIR region of the 2×2 TIR TO switch element. The inset in Fig. 1(b) shows the mode field distribution of the 3μm-wide waveguide. WG: waveguide.

TABLE I

OPTIMIZED OR SELECTED PARAMETERS AT 1550 nm AND 298 K

Material	Parameter value				
	RI	TC ($WK^{-1}m^{-1}$)	ALC (cm^{-1})	ρ (kg/m^3)	c_p (J/kg·K)
SU-8	1.5742	0.20	0.22	1190	1200
P(MMA-GMA)	1.4798	0.19	0.65	1190	1420
Silica	1.4440	1.40	≈0	2200	730
Gold	0.19	317	2.47×10^5	19302	130

Structural parameter	Value	Structural parameter	Value
Slab thickness	2.0μm	Waveguide width a_2	40.0μm
Rib height	1.0μm	Waveguide width W_{cross}	40.1μm
Silica layer thickness	2.0μm	Waveguide gap d_1	250μm
PMMA layer thickness	3.0μm	Heater electrode width d_2	10.0μm
Waveguide width a_1	3.0μm	Half crossing angle α	3.5°

RI: refractive index; TC: thermal conductivity; ALC: amplitude loss coefficient

The waveguide width is taken as $a_1 = 3.0$ μm for single-mode propagation. The mode amplitude loss is estimated to be 0.23 cm^{-1}, corresponding to a power loss of about 0.46 cm^{-1}. The mode field distribution is shown in the inset of Fig. 1(b).

Figs. 2(b) and 2(c) show the effects of waveguide width a_2 on the crosstalk and propagation loss of the device under "through" state (heater temperature increase $\Delta T = 0$ K) and "reflection" state ($\Delta T = 50$ K). For obtaining both a low loss (< 4 dB) and a low crosstalk (<−40 dB), a relatively wide waveguide ($a_2 > 40.0$ μm) is required. Though such a wide waveguide supports multimode propagation, the input/output waveguides assure the injection and ejection of single-mode light.

C. Crossing Angle Optimization

The three horizontal lengths related to the TIR region are designed to be $L_2 = 3460$ μm, $L_{21} = 1485$ μm, and $L_{22} = 490$ μm. The distance between two input (or output) waveguides is $d_1 = 250$ μm. Given the half crossing angle α, we can decide the radius R and horizontal length L_1 of the arc-bending waveguide in the transition regions as

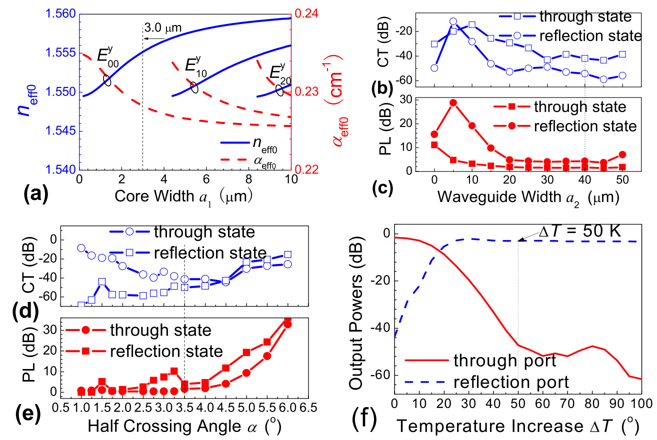

Fig. 2. (a) Effective refractive index (n_{eff0}) and mode amplitude loss coefficient (α_{eff0}) as a function of core width (a_1) of the three high-order modes for the input/output waveguides. (b) Crosstalk (CT) and (c) propagation loss (PL) under "through" and "reflection" states as a function of a_2. (d) Crosstalk (CT) and (e) propagation loss (PL) under "through" and "reflection" states as a function of half crossing angle (α). (f) Output powers from the through and reflection ports as a function of the temperature increase of the heater.

$$R = L_1/\sin\alpha, \quad R(1-\cos\alpha) + L_2\tan\alpha/2 = d_1/2. \quad (1)$$

This relation will be used in the structure design of the switch. Under "reflection" and "through" states, Figs. 2(d) and 2(e) show the effects of α on the crosstalk and propagation loss of the switch. It can be observed that a very large α will lead to a significant increase of propagation loss and crosstalk. A very small α will lead to the increase of crosstalk at "through" state. Therefore, we choose $\alpha = 3.5^o$. The related propagation losses at both states are <4 dB and <1.6 dB, respectively. The crosstalk also drops to a relatively low level (<−40 dB).

D. Simulation on Switching Function

The heat distribution over the waveguide cross-section can be obtained by solving the following equation [11]

$$k\nabla^2 T(x, y, t) + q(x, t) = \rho c_p \partial T(x, y, t)/\partial t, \quad (2)$$

where T is the temperature distribution, t is the time, k is the thermal conductivity, q is the heat power per unit volume applied through the heater at $y = 0$, ρ is the material density, and c_p is the specific heat. The material mass density and specific heat are listed in Table I. After heating the electrode ($\Delta T = 50$ K), the refractive index change distribution over the waveguide cross-section in Fig. 1(c) is shown in Fig. 3(a). In this case, the wide waveguide is divided into two sub-waveguides, e.g. left waveguide (LW) and right waveguide (RW). The effective width of the two high-index regions is about 20 μm, and the effective thickness of the low-index region is about 5 μm. The incident light into the cross-point will be reflected by the low-index region and will propagate into the reflection port. Under different ΔT values, the effective width and thickness of the formed high- and low-index regions are different, leading to different output powers. The effects of temperature increase on the output powers are shown in Fig. 2(f). As ΔT increases, more power will

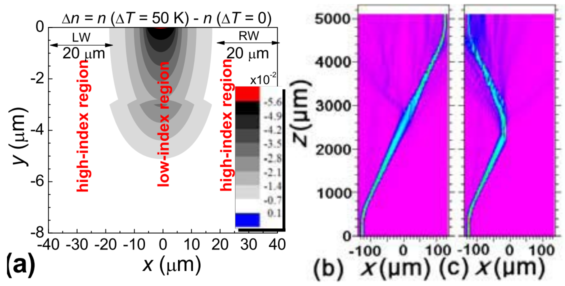

Fig. 3. (a) Refractive index change distribution over the cross-section in Fig. 1(c) upon $\Delta T = 50$ K. (b), (c) Propagation powers of the TIR switch under (b) "through" state ($\Delta T = 0$ K) and (c) "reflection" state ($\Delta T = 50$ K).

be injected into the "reflection" port. When $\Delta T = 50$ K, the switch can be switched from "through" to "reflection" state. When ΔT equals 0 K and 50 K, the simulated propagation powers along the waveguides are shown in Figs. 3(b) and 3(c). Good switching performances are observed for the element. The final optimized structural parameters are listed in Table I.

III. Device Fabrication and Measurements

A. Fabrication

A 2.0μm-thick silica layer was grown on the silicon substrate as an under cladding. Then, a 3.0 μm SU-8 2005 layer was spun-coated on the under cladding. After soft bake (5 min), the rib waveguides with a rib height of 1.0 μm was formed by photolithography technique and wet etching process. Furthermore, the core film was hard-baked to sufficiently cross-link the material. Finally, a 3.0μm-thick P(MMA-GMA) film was spun-coated to form the upper cladding.

Upon the upper cladding, a 100nm-thick gold layer was deposited through thermal evaporation. Then, a positive photoresist (BP218) was spun-coated (4000 rpm) and baked at 90 °C for 1 min. The sample was cooled down to room temperature naturally. The coated wafer was contact-exposed under UV radiation using an electrode mask for 8.5 s. The sample was developed in the NaOH solution with a concentration of 5‰. Finally, by using a photoresist stripper, we removed all the photoresist. A 10.0μm-wide and ~1mm-long thin-film gold heater was formed.

The photograph of the final fabricated 4.0cm-long switch element is shown in Fig. 4(a). The device to be tested is shown in the red rectangular box. The detailed illustration in the cross waveguide region is exhibited in Fig. 4(b), where two cross waveguides can be obviously observed.

B. Measurements

An input power of 0 dBm was coupled into port A with 1550 nm wavelength. The electrical driving signal was supplied to the heater pads (see Fig. 4(a)) through two microwave probes. By changing the supply voltage, we tuned the driving power. By using an optical power meter, we measured the two output powers (P_{AC}, P_{AD}), as shown in Fig. 5(a). When the driving power equals 0 mW ("through" state), P_{AC} and P_{AD} are -39.2 and -15.0 dBm, respectively. The total propagation loss and crosstalk are about 15.0 and -24.2 dB, respectively. The measured far-field pattern of the two output light beams is shown in Fig. 4(c). As the driving power increases, the output powers of the two output ports change in an opposite manner. When the driving power is >76 mW, P_{AC} and P_{AD} are >-16.8 dBm and <-38.4 dBm, respectively, which is "reflection" state, and the total propagation loss and crosstalk are about 16.8 and -21.6 dB, respectively. The measured far-field pattern is shown in Fig. 4(d) under this state.

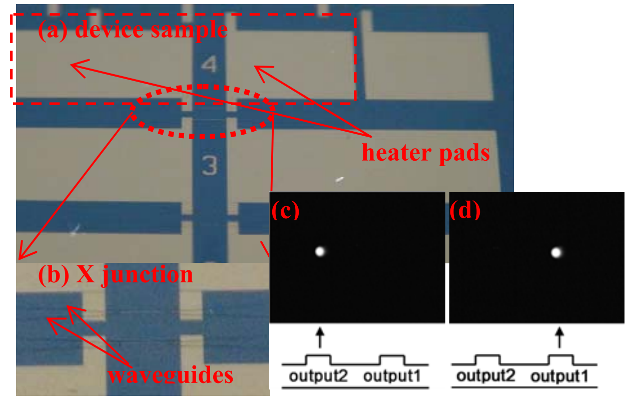

Fig. 4. (a) Photograph of the fabricated TIR TO switch, and (b) photograph of the fabricated X junction waveguide. The measured far-field patterns of each of the two output light beams under (c) "through" state and (d) "reflection" state.

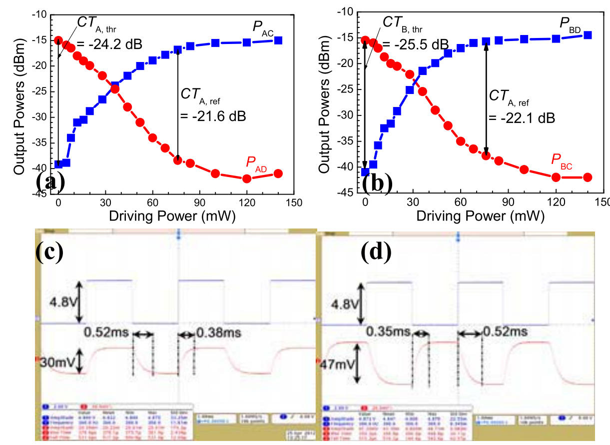

Fig. 5. (a) Measured output powers (P_{AC}, P_{AD}) over driving power. (b) Measured output powers (P_{BC}, P_{BD}) over driving power. *CT*: crosstalk. (c), (d) Measured modulation responses of the output powers (c) P_{AC} and (d) P_{AD}. The upper trace is the driving voltage signal. The lower trace is the response signal.

Similar experiment was done when the light was input-coupled into port B, as shown in Fig. 5(b). Subtracting the measured fiber-to-chip coupling loss (3 dB per connection) and the transmission loss of input/output waveguides (7.2 dB) from the total loss (15.0 dB at "through" state and 16.8 dB at "reflection" state), we obtain the through loss (IL_{thr}) and reflection loss (IL_{ref}) to be about 1.8 dB and 3.6 dB, respectively, for the 0.47cm-long core switch element.

Under 300 Hz switching operation, the dynamic variation curves of P_{AC} and P_{AD} are shown in Fig. 5(c) and Fig. 5(d), respectively. The measured rise time and fall time of the TIR switch are about 0.35/0.38 and 0.52 ms, respectively. Because the needed heat accumulation in the waveguide is significantly larger than that of the phase-change-based

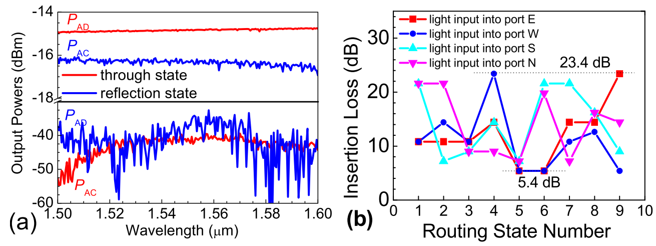

Fig. 6. (a) Spectral characteristics of the TIR switch element. (b) Propagation loss characteristics under all routing operations for the TIR optical router.

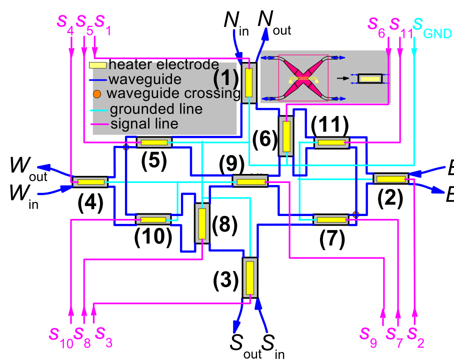

Fig. 7. Topology of the non-blocking four-port optical router. The input and output of a specific port are arranged in the same physical address. s_i is the driving signal line for the i-th element; s_{GND} is the grounded line.

TABLE II

NON-BLOCKING ROUTING OPERATIONS AND PATHS OF THE ROUTER

		Input				Operation state of switch elements										
		E_i	W_i	S_i	N_i	1	2	3	4	5	6	7	8	9	10	11
1	output	N_o	S_o	W_o	E_o	r	r	r	r	r	t	r	t	r	t	t
2	output	N_o	E_o	W_o	S_o	r	r	t	t	r	t	r	t	t	t	t
3	output	N_o	S_o	E_o	W_o	r	r	r	r	t	t	t	t	t	t	t
4	output	S_o	E_o	N_o	W_o	r	r	t	r	t	r	r	r	t	t	t
5	output	S_o	N_o	W_o	E_o	t	t	t	t	t	t	t	t	t	t	t
6	output	S_o	N_o	E_o	W_o	t	t	t	t	t	r	t	r	r	t	t
7	output	W_o	S_o	N_o	E_o	t	t	r	r	r	t	r	t	t	t	t
8	output	W_o	E_o	N_o	S_o	r	t	r	r	r	t	r	t	t	r	r
9	output	W_o	N_o	E_o	S_o	t	r	r	t	t	r	t	r	t	t	t

Note: "t" represents "through" state; "r" represents "reflection" state.

MZI TO switch [12], the rise/fall times are both longer than those of the device (<0.1 ms) fabricated with the same silica/polymer materials in [12].

An experiment was performed to investigate the spectral characteristics of such kind of switch by tuning the wavelength within 1.5∼1.6 μm, as shown in Fig. 6(a). The device exhibits wavelength insensitive characteristics with small variation of output power from the "on" port and <−38 dBm output power from the "off" port.

IV. A FOUR-PORT OPTICAL ROUTER AND TOPOLOGY

A four-port optical router using 11 TIR TO switch elements is proposed, as shown in Fig. 7, where two waveguide crossings are required. The switch elements are numbered from 1 to 11. The routing operations (with 9 states) are summarized in Table II. The router can realize exactly non-blocking operation, which is highly required in a chip-level multiprocessors-based optical NoC. Besides, in the topology, the four ports are naturally positioned in the same physical address, which is also demanded in constructing large-scale optical NoCs using non-blocking optical routers.

Under all routing states, the propagation loss characteristics when the light is input-coupled into ports E, W, S and N are summarized in Fig. 6(b). Under most routing operations, the propagation losses are 5.4∼23.4 dB.

Another consideration is the power consumption of the router. For achieving −10 dB crosstalk, a power consumption of 50 mW ("r" state) is required for one switch element. Based on Table II, within all operations, the minimum and maximum numbers of the switch elements at "r" states are 0 and 7, respectively, and thus an average power consumption of 175 mW is needed. This value is higher than those of the four-port MRR routers in [2] and [4] (20∼50 mW), due to the adopted TIR effect other than the phase-change-induced effect.

One drawback of the router is that it has more elements compared with the routing models in [2]–[4], [7], and [8], where 4∼8 switch elements were adopted in general. However, the proposed topology, the TIR element and the wide spectrum properties make the router different from the reported schemes.

V. CONCLUSION

In summary, we demonstrated a silica/polymer TIR TO switch. A switching power of 70 mW is required to drop the crosstalk below −20 dB. The 10–90% rise time and 90–10% fall time are 0.35 and 0.52 ms, respectively. By using 11 switch elements, we proposed a non-blocking four-port optical router, whose propagation loss range is 5.4–23.4 dB for all routing paths. The router has potential applications of signal switching and routing in a multiprocessors-based optical NoC.

REFERENCES

[1] A. W. Poon, X. Luo, F. Xu, and H. Chen, "Cascaded microresonator-based matrix switch for silicon on-chip optical interconnection," *Proc. IEEE*, vol. 97, no. 7, pp. 1216–1238, Jul. 2009.

[2] A. Biberman, B. G. Lee, N. Sherwood-Droz, M. Lipson, and K. Bergman, "Broadband operation of nanophotonic router for silicon photonic networks-on-chip," *IEEE Photon. Technol. Lett.*, vol. 22, no. 12, pp. 926–928, Jun. 15, 2010.

[3] M. Yang *et al.*, "Non-blocking 4 × 4 electro-optic silicon switch for on-chip photonic networks," *Opt. Exp.*, vol. 19, no. 1, pp. 47–54, 2011.

[4] R. Ji *et al.*, "Microring-resonator-based four-port optical router for photonic networks-on-chip," *Opt. Exp.*, vol. 19, no. 20, pp. 18945–18955, 2011.

[5] R. Ji *et al.*, "Five-port optical router for photonic networks-on-chip," *Opt. Exp.*, vol. 19, no. 21, pp. 20258–20268, 2011.

[6] R. Ji, J. Xu, and L. Yang, "Five-port optical router based on microring switches for photonic networks-on-chip," *IEEE Photon. Technol. Lett.*, vol. 25, no. 5, pp. 492–495, Mar. 1, 2013.

[7] R. Min, R. Ji, Q. Chen, L. Zhang, and L. Yang, "A universal method for constructing n-port nonblocking optical router for photonic networks-on-chip," *J. Lightw. Technol.*, vol. 30, no. 23, pp. 3736–3741, Dec. 1, 2012.

[8] Q. Chen, F. Zhang, R. Ji, L. Zhang, and L. Yang, "Universal method for constructing N-port non-blocking optical router based on 2 × 2 optical switch for photonic networks-on-chip," *Opt. Exp.*, vol. 22, no. 10, pp. 12614–12627, 2014.

[9] C. T. Zheng, L. Liang, Q. Q. Luo, C. S. Ma, D. M. Zhang, and Y. D. Wang, "Microring-based $N \times N$ scalable polymeric electrooptic routing switch array: Theory, architecture, and design scheme," *IEEE Photon. J.*, vol. 5, no. 3, Jun. 2013, Art. ID 7200620.

[10] C. T. Zheng, Q. Q. Luo, X. L. Huang, and D. M. Zhang, "Multifunctional polymer Mach–Zehnder optical switch/filter using side-coupled $M \times N$ electrooptic microring array," *IEEE Photon. J.*, vol. 6, no. 4, Aug. 2014, Art. ID 2332459.

[11] W.-K. Wang, H. J. Lee, and P. J. Anthony, "Planar silica-glass optical waveguides with thermally induced lateral mode confinement," *J. Lightw. Technol.*, vol. 14, no. 3, pp. 429–436, Mar. 1996.

[12] L. Liang *et al.*, "Low-power and high-speed thermo-optic switch using hybrid silica/polymer waveguide structure: Design, fabrication and measurement," *J. Modern Opt.*, vol. 59, no. 12, pp. 1084–1091, 2012.